



Contents lists available at ScienceDirect

## Journal of Quantitative Spectroscopy &amp; Radiative Transfer

journal homepage: [www.elsevier.com/locate/jqsrt](http://www.elsevier.com/locate/jqsrt)

# Enhancement, suppression of the emission and the energy transfer by using a graphene subwavelength wire

Mauro Cuevas<sup>a,b,\*</sup>

<sup>a</sup> Consejo Nacional de Investigaciones Científicas y Técnicas (CONICET) and Facultad de Ingeniería y Tecnología Informática, Universidad de Belgrano, Villanueva 1324, C1426BMJ, Buenos Aires, Argentina

<sup>b</sup> Grupo de Electromagnetismo Aplicado, Departamento de Física, FCEN, Universidad de Buenos Aires and IFIBA, Ciudad Universitaria, Pabellón I, C1428EHA, Buenos Aires, Argentina



## ARTICLE INFO

## Article history:

Received 17 February 2018

Revised 7 April 2018

Accepted 18 April 2018

Available online 21 April 2018

## Keywords:

Surface plasmon

Graphene

Spontaneous emission

Dipole–dipole interaction

## ABSTRACT

The present work focuses on theoretically research on the spontaneous emission and the energy transfer process between two single optical emitters placed close to a graphene coated wire. The localized surface plasmons (LSPs) supported by the structure provide decay channels which lead to an enhancement of the emission and radiation decay rates as well as an improvement in the energy transfer between two dipole emitters. Modifications resulting from varying the orientation of dipole moments in these quantities are shown. We find that the radiation and the energy transfer efficiencies can be largely reduced at a specific frequency depending on the emitter location. By dynamically tuning the chemical potential of graphene coating, the spectral region where the dipole–field interaction is enhanced can be chosen over a wide range.

© 2018 Elsevier Ltd. All rights reserved.

## 1. Introduction

It is known that the radiation characteristics of a quantum emitter (atom, molecule, quantum dots or wires) depends on the environment [1], and the spontaneous emission can be controlled by modifying the photonic density of states to the oscillating dipole [2]. A way to achieve this effect consists of coupling the quantum emitter to resonant optical modes, like wave guiding or surface plasmon (SP) modes, which provide new channels to selectively increase the emission rate into these modes [3–7].

The range of the quantum emitters interaction can also be enhanced by coupling these emitters to a designed wave guiding or SP mode environments. A variety of structures such as uniform planar microcavities [8], cylindrical nanowires [9] nanowaveguides [10] and metal films [11] have been the object of intensive research over the last few years due to the possibility to engineer wave guiding or SP mode distributions to mediate the energy transfer between quantum emitters.

High radiative quantum efficiency, large spontaneous emission rate and efficient light energy transfer are some of the main features to achieve practical nanophotonic devices, such as nanoscale

antennas [3,4,12] and references therein), plasmon lasers [13] and photon–plasmon coupler nanostructures [14,15].

The advent of graphene, which offers electrically tunable, low loss and highly confined SPs [16–18], has widened possibilities to light control in a wide frequency range allowing the movement of metal plasmonic applications, currently working in the visible range, to the mid–infrared and terahertz frequencies [19–22]. Special phase matching techniques, such as prism or grating coupling, extensively used in the metallic and metamaterial case [23–26], have been considered involving graphene in Refs. [27–30]. In addition, the improvement of the spontaneous emission of a quantum emitter close to a graphene sheet and the possibility to control the strength of the interaction between two emitters placed in the vicinity of the sheet [31,32], has aroused a particular interest in studying other geometries that include graphene [33–37].

In this paper we consider a cylindrical dielectric core of circular cross section coated with a graphene layer. In this context, we have focused on the influence that the SPs play in the emission characteristics and the optical interaction between two line dipole emitters in close proximity to a graphene wire.

In a previous work [38] we investigated the emission and radiation properties of a single emitter placed inside a graphene coated cylinder. Unlike the results found in this work, in the present contribution we find radiation spectra highly depending on the orientation of the emitter dipole moment. In addition, both the resonant enhancements as well as a significant reduction in the power

\* Correspondence to: Consejo Nacional de Investigaciones Científicas y Técnicas (CONICET) and Facultad de Ingeniería y Tecnología Informática, Universidad de Belgrano, Villanueva 1324, C1426BMJ, Buenos Aires, Argentina.

E-mail address: [cuevas@df.uba.ar](mailto:cuevas@df.uba.ar)

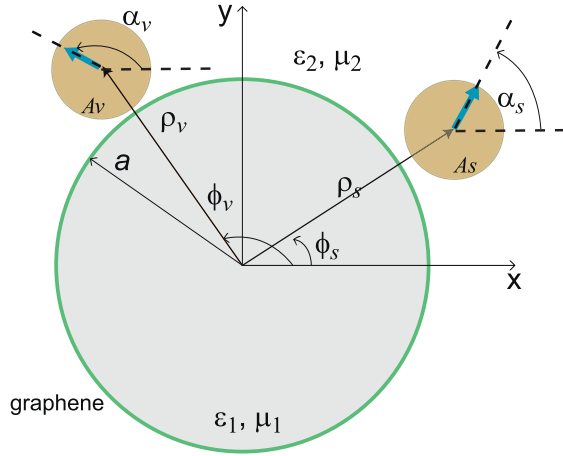


Fig. 1. Schematic illustration of the system.

radiated by the emitter have been found. Curiously, as its active media counterpart [39] the graphene coated wire has the ability to enhance the radiated power by an emitter in proximity to it as well as to reduce at near zero values this power. We also find large enhancements in the energy transfer between line dipole emitters which can be controlled by electrical tuning of the plasmon resonances.

This paper is organized as follows. First, in Section 2 we sketch the boundary–value problem for the diffraction of a wave emitted by an oscillating dipolar line source placed in close proximity to a dielectric cylinder wrapped with a graphene sheet and derive analytical expressions for the emitted and radiated power efficiencies. We then include a second dipolar line source and briefly deal with the problem of the coupled system, providing a known expression to calculate the energy transfer between two dipoles. In Section 3 we present the examples analyzing the magnitude of the radiation efficiency as well as the energy transfer decay rate. Finally, concluding remarks are provided in Section 4. The Gaussian system of units is used and an  $\exp(-i\omega t)$  time-dependence is implicit throughout the paper, with  $\omega$  as the angular frequency,  $t$  as the time, and  $i = \sqrt{-1}$ . The symbols Re and Im are respectively used for denoting the real and imaginary parts of a complex quantity.

## 2. Theory

### 2.1. Electromagnetic field scattered by a line dipolar source

We consider a graphene coated cylinder with circular cross section (radius  $a$ ) centered at  $x = 0$ ,  $y = 0$  (Fig. 1). The wire substrate is characterized by the electric permittivity  $\epsilon_1$  and the magnetic permeability  $\mu_1$ . The coated wire is embedded in a transparent medium with electric permittivity  $\epsilon_2$  and magnetic permeability  $\mu_2$ . A two dimensional emitter (a line dipole source whose axis lies along the  $\hat{z}$  axis) with a dipole moment  $\vec{p}_s = p(\cos \alpha \hat{x} + \sin \alpha \hat{y})$  is placed outside the cylinder, at position  $\vec{r}_s = \rho_s \hat{\rho} + \phi_s \hat{\phi}$  ( $\rho_s > a$ ). The dipole is aligned at an angle  $\alpha_s$  with respect to the  $\hat{x}$  axis, as indicated in Fig. 1. The current density of the electric dipole is

$$\vec{j}_s(\vec{r}) = -i\omega \vec{p}_s \delta(\vec{r} - \vec{r}_s) = -i\omega \vec{p}_s \frac{1}{\rho} \delta(\rho - \rho_s) \delta(\phi - \phi_s). \quad (1)$$

In an unbounded medium 2 the dipole fields are obtained from the vector potential  $\vec{A}$  [38],

$$\vec{A}(\rho, \phi) = \sum_{m=-\infty}^{+\infty} \pi k_0 J_m(k_2 \rho_<) H_m^{(1)}(k_2 \rho_>) e^{im(\phi - \phi_s)} \times [p_\rho \hat{\rho} + p_\phi \hat{\phi}], \quad (2)$$

$$\vec{H}(\rho, \phi) = \nabla \times \vec{A} = \hat{z} \varphi(\rho, \phi), \quad (3)$$

$$\vec{E}(\rho, \phi) = \frac{i}{k_0 \epsilon_2} \nabla \times \vec{H}(\rho, \phi) = -\frac{i}{k_0 \epsilon_2} \hat{z} \times \nabla_t \varphi, \quad (4)$$

where  $\varphi(\rho, \phi)$  is the non-zero component of the total magnetic field along the axis of the wire ( $\hat{z}$  axis),  $\nabla_t = \hat{\rho} \frac{\partial}{\partial \rho} + \hat{\phi} \frac{1}{\rho} \frac{\partial}{\partial \phi}$  is the transverse part of the  $\nabla$  operator,  $k_0 = \omega/c$  is the modulus of the photon wave vector in vacuum,  $\omega$  is the angular frequency,  $c$  is the vacuum speed of light,  $\rho_<$  ( $\rho_>$ ) is the smaller (larger) of  $\rho$  and  $\rho_s$ ,  $p_\rho$  and  $p_\phi$  are the projection of vector  $\vec{p}_s$  on the  $\hat{\rho}$  and  $\hat{\phi}$  axis, respectively, and  $J_m$  and  $H_m^{(1)}$  are the  $n$ th Bessel and Hankel functions of the first kind, respectively. From Eqs. (2) and (3), we obtain the primary magnetic field emitted by the dipole,

$$\varphi_i(\rho, \phi) = \sum_{m=-\infty}^{+\infty} \pi k_0 k_2 J_m(k_2 \rho_s) \times \left[ H_m^{(1)'}(k_2 \rho) p_\theta - im \frac{H_m^{(1)}(k_2 \rho)}{k_2 \rho} p_\rho \right] e^{im(\phi - \phi_s)}, \quad (5)$$

for  $\rho > \rho_s$ , and

$$\varphi_i(\rho, \phi) = \sum_{m=-\infty}^{+\infty} \pi k_0 k_2 H_m^{(1)}(k_2 \rho_s) \times \left[ J_m'(k_2 \rho) p_\theta - im \frac{J_m(k_2 \rho)}{k_2 \rho} p_\rho \right] e^{im(\phi - \phi_s)}, \quad (6)$$

for  $\rho < \rho_s$ .

The scattered magnetic field along the axis of the wire, i.e., the  $\hat{z}$  component, denoted by  $\varphi_{sc}^{(j)}$  ( $j = 1, 2$ ), is expanded as a series of cylindrical harmonics, one for the internal region ( $\rho < a$ ),

$$\varphi_{sc}^{(1)}(\rho, \phi) = \sum_{m=-\infty}^{+\infty} a_m J_m(k_1 \rho) e^{im\phi}, \quad (7)$$

and another one for the external region ( $\rho > a$ ),

$$\varphi_{sc}^{(2)}(\rho, \phi) = \sum_{m=-\infty}^{+\infty} b_m H_m^{(1)}(k_2 \rho) e^{im\phi}, \quad (8)$$

where  $a_m$  and  $b_m$  are unknown complex coefficients. The boundary conditions for the graphene-coated cylinder at  $\rho = a$  can be expressed as [38]

$$\frac{1}{\epsilon_1} \frac{\partial}{\partial \rho} \varphi_{sc}^{(1)}|_{\rho=a} = \frac{1}{\epsilon_2} \frac{\partial}{\partial \rho} (\varphi_i + \varphi_{sc}^{(2)})|_{\rho=a}, \quad (9)$$

and

$$(\varphi_i + \varphi_{sc}^{(2)})|_{\rho=a} - \varphi_{sc}^{(1)}|_{\rho=a} = \frac{4\pi\sigma}{ck_0\epsilon_1} i \frac{\partial}{\partial \rho} \varphi_{sc}^{(1)}|_{\rho=a}. \quad (10)$$

By inserting the expressions (5), (7) and (8) into the boundary conditions, the amplitudes of the scattered field can be written as

$$a_m = f_m(y_s) \tilde{a}_m, \quad (11)$$

$$b_m = f_m(y_s) \tilde{b}_m, \quad (12)$$

where

$$f_m(y_s) = \frac{k_0 k_2 p}{2i} \times [H_{m+1}(y_s) e^{i(\alpha - \phi_s)} + H_{m-1}(y_s) e^{-i(\alpha - \phi_s)}] e^{-im\phi_s}, \quad (13)$$

$$\tilde{a}_m = \frac{k_2 \varepsilon_1 [J_m(y) H'_m(y) - H_m(y) J'_m(y)]}{k_2 \varepsilon_1 J_m(x) H'_m(y) - k_1 \varepsilon_2 J'(x) H_m(y) + \frac{4\pi\sigma}{ck_0} ik_1 k_2 J'_m(x) H'_m(y)}, \quad (14)$$

$$\tilde{b}_m = \frac{[k_1 \varepsilon_2 J_m(y) J'_m(x) - k_2 \varepsilon_1 J'_m(y) J_m(x) - \frac{4\pi\sigma}{ck_0} ik_1 k_2 J'_m(x) J'_m(y)]}{k_2 \varepsilon_1 J_m(x) H'_m(y) - k_1 \varepsilon_2 J'(x) H_m(y) + \frac{4\pi\sigma}{ck_0} ik_1 k_2 J'_m(x) H'_m(y)} \quad (15)$$

and  $x = k_1 a$ ,  $y = k_2 a$ ,  $y_s = k_2 \rho_s$  and the prime denotes the derivative with respect to the argument.

## 2.2. Emission and radiation properties

According to Poynting theorem, the time-averaged power  $P$  emitted by the dipole coupled to the graphene wire can be calculated from the integral of the normal component of the complex Poynting vector flux through an imaginary cylinder of length  $L$  and surface  $A_s$  that encloses the dipole (see Fig. 1)

$$P = -\frac{1}{2} L \int_{A_s} \text{Re} \{ \vec{j}_s^* \cdot \vec{E} \} da, \quad (16)$$

where  $A_s$  encloses the source,  $da = \rho_s d\phi_s d\rho_s$  and  $\vec{j}_s$  represents the source density current. Introducing the value of the current in Eq. (1) and taking into account that  $\vec{E} = \vec{E}_{inc} + \vec{E}_s$ , where  $\vec{E}_{inc}$  and  $\vec{E}_s$  are the primary dipole field and the scattered field, respectively, we obtain

$$P = \frac{\omega L}{2} \text{Im} \{ \vec{p}_s \cdot \vec{E}_{inc}(\rho_s, \phi_s) \} + \frac{\omega L}{2} \text{Im} \{ \vec{p}_s \cdot \vec{E}_s(\rho_s, \phi_s) \}. \quad (17)$$

Inserting the values of  $\vec{E}_{inc}$  and  $\vec{E}_s$ , both fields calculated by using Eqs. (4), (5) and (8), into Eq. (17) we obtain

$$P = P_{inc} - \frac{cL}{\varepsilon_2} \times \text{Im} \left\{ \sum_{m=-\infty}^{+\infty} b_m [p_\rho m k_2 \frac{H_m(y_s)}{y_s} + ip_\phi k_2 H'_m(y_s)] e^{im\phi_s} \right\}, \quad (18)$$

where  $P_{inc} = \frac{\pi k_0^3 p^2 c L}{4}$  is the total power emitted by an electric dipole in the unbounded medium 2 [38].

Similarly, the time-averaged power radiated by the emitter can be evaluated by calculating the complex Poynting vector flux through an imaginary cylinder of length  $L$  and radius  $\rho_1 > \rho_s$  that encloses the source

$$P_{sc} = \frac{c}{8\pi} L \int_0^{2\pi} \text{Re} \{ \vec{E} \times \vec{H}^* \} \cdot \hat{r} \\ = \frac{\rho_1 L c^2}{8\pi \omega \varepsilon_2} \int_0^{2\pi} \text{Re} \left\{ -i [\varphi_{inc} + \varphi_s^{(2)}]^* \frac{\partial}{\partial \rho} [\varphi_{inc} + \varphi_s^{(2)}] \right\} d\phi. \quad (19)$$

In the far-field region the calculation of both the primary and the scattered fields given by Eqs. (6) and (8) can be greatly simplified using the asymptotic expansion of the Hankel function for large argument [40]. After some algebraic manipulation, we obtain

$$P_{sc} = P_{inc} + \frac{L c^2}{2\pi \omega \varepsilon_2} \sum_{m=-\infty}^{+\infty} |b_m|^2 \\ + \frac{c k_2 p L}{2\varepsilon_2} \sum_{m=-\infty}^{+\infty} J_m(y_s) \text{Im} \{ b_{m-1}^* e^{i(\alpha - m\phi_s)} + b_{m+1}^* e^{-i(\alpha + m\phi_s)} \}. \quad (20)$$

To quantitatively characterize the effect of the graphene coating, we define the normalized spontaneous emission rate  $F$  as the ratio between the power emitted by the dipole, given by Eq. (18), and the power  $P_{inc}$  emitted by the same dipole embedded in an unbounded medium 2. In a similar way, the radiative efficiency  $F_{sc}$  is defined as the ratio between the power radiated by the dipole, given by Eq. (20), and the power emitted by the dipole in the unbounded medium 2.

## 2.3. Resonant energy transfer

In this section we focus on the interaction between two line dipole emitters, with electric dipole moments  $\vec{p}_s$  and  $\vec{p}_v$ , and equal transition frequency  $\omega$ , and placed outside the graphene-wire (inside medium 2). According with Poynting theorem the time-average power transferred from the dipole  $\vec{p}_s$  (donor) to dipole  $\vec{p}_v$  (acceptor) can be calculated by

$$P_{ET} = -\frac{1}{2} L \int_{A_v} \text{Re} \{ \vec{j}_v^* \cdot \vec{E}_s \} da, \quad (21)$$

where  $A_v$  encloses the acceptor dipole  $v$ ,  $da = \rho_v d\phi_v d\rho_v$ ,  $\vec{j}_v$  represents the source density current associated with the dipole  $v$  and  $\vec{E}_s$  is the electric field generated by the donor dipole  $s$  [41]. In this approximation, the current density  $\vec{j}_v$  reads as in Eqs. (1) and (21) can be written as

$$P_{ET} = \frac{\omega L}{2} \text{Im} \{ \vec{p}_v \cdot \vec{E}_s(\rho_v, \phi_v) \}. \quad (22)$$

Taking into account that the dipole moment  $\vec{p}_v$  is the induced dipole by the  $\vec{E}_s$  field generated by  $\vec{p}_s$ , in the linear regime we obtain [41]

$$P_{ET} = \frac{\omega L}{2} \text{Im} \{ \alpha_v \} |\hat{n}_v \cdot \vec{E}_s(\rho_v, \phi_v)|^2, \quad (23)$$

where  $\alpha_v$  is the polarizability of the acceptor and  $\hat{n}_v$  is a unit vector along the induced polarization of the acceptor (whose direction is supposedly to be fixed). The energy transfer rate in the presence of the graphene-wire normalized to that in medium 2 (without graphene-wire), is given by

$$F_{ET} = \frac{|\hat{n}_v \cdot \vec{E}_s(\rho_v, \phi_v)|^2}{|\hat{n}_v \cdot \vec{E}_s^{(0)}(\rho_v, \phi_v)|^2}, \quad (24)$$

where  $\vec{E}_s^{(0)}(\rho_v, \phi_v)$  is the field generated by the donor at position of the acceptor in absence of the graphene-wire. It is worth noting that the graphene coating introduces LSP mechanisms, absent in the bare wire, which are able to enhance the field  $\vec{E}_s$  emitted by the donor in an environment of the wire at resonance frequencies. Thus, when the acceptor dipole is placed in the vicinity of the wire, the numerator in Eq. (24), and thus the energy transfer  $F_{ET}$ , is enhanced at resonant frequencies. In this way, given the plasmonic field enhancement in the graphene coating, an important improvement in the energy transfer between donor and acceptor is expected.

## 3. Results

In this section we apply the formalism sketched in previous sections to calculate the spontaneous emission and the energy transfer rates for dipole emitters in the presence of a graphene-wire. We assume that radius  $a$  is sufficiently large as to describe the optical properties of the wire as those of a circular cylinder characterized by the same surface conductivity as planar graphene [42].

Based on the complete description of experimental observations by the zero-thickness interface model [43], we consider the

**Table 1**

Complex roots  $\omega_n/c$  of the denominator of  $a_m$  and  $b_m$  in (11) and (12),  $a = 30$  nm,  $\gamma_c = 0.1$  meV,  $\varepsilon_1 = 2.13$ ,  $\mu_1 = 1$ ,  $\varepsilon_2 = 1$ ,  $\mu_2 = 1$ .

$m$	1	2
$\mu_c = 0.5$ eV	$0.8868 - i4.105 \cdot 10^{-4}$	$1.2547 - i2.5321 \cdot 10^{-4}$
$\mu_c = 0.75$ eV	$1.0859 - i5.4207 \cdot 10^{-4}$	$1.5365 - i2.5332 \cdot 10^{-4}$
$\mu_c = 1$ eV	$1.2535 - i6.9772 \cdot 10^{-4}$	$1.7741 - i \cdot 10^{-4}$

graphene layer as an infinitesimally thin, local and isotropic two-sided layer with frequency-dependent surface conductivity  $\sigma(\omega)$  given by the Kubo formula [44,45], which can be read as  $\sigma = \sigma^{intra} + \sigma^{inter}$ , with the intraband and interband contributions being

$$\sigma^{intra}(\omega) = \frac{2ie^2k_B T}{\pi \hbar(\omega + i\gamma_c)} \ln[2\cosh(\mu_c/2k_B T)], \quad (25)$$

$$\sigma^{inter}(\omega) = \frac{e^2}{\hbar} \left\{ \frac{1}{2} + \frac{1}{\pi} \arctan[(\omega - 2\mu_c)/2k_B T] - \frac{i}{2\pi} \ln \left[ \frac{(\omega + 2\mu_c)^2}{(\omega - 2\mu_c)^2 + (2k_B T)^2} \right] \right\}, \quad (26)$$

where  $\mu_c$  is the chemical potential,  $\gamma_c$  the carriers scattering rate,  $e$  the electron charge,  $k_B$  the Boltzmann constant and  $\hbar$  the reduced Planck constant.

The dependence of the chemical potential  $\mu_c$  on the external electric field can be expressed as  $\mu_c = \frac{1}{\pi(\hbar v_F)^2} \int_0^\infty \epsilon [f(\epsilon - \mu_c) - f(\epsilon + \mu_c)] d\epsilon \approx \text{sgn}(n_s) \hbar v_F \sqrt{\pi |n_s|}$  [46], where the last equality is valid for  $\mu_c$  values large enough that  $k_B T$  (large doping condition),  $v_F = 10^8$  cm/s is the Fermi velocity,  $f(x)$  is the Fermi function with chemical potential  $\mu_c$ ,  $n_s = E(a)/(4\pi e)$  is the charge density and  $E(a)$  is the modulus of the electric field at the graphene surface. The electric field outside the cylinder  $E(r) = \frac{4\pi n_s e a}{r}$  ( $E(r) = \frac{n_s e a}{\epsilon_0 r}$  in the international system (SI)). For instance, a value of 1 eV for the chemical potential corresponds to an electric field  $E = 1.33$  MV/cm at the graphene surface.

In all the calculations we have used  $\gamma_c = 0.1$  meV, the core (radius  $a = 30$  nm) is made of a transparent material with constitutive parameters  $\varepsilon_1 = 2.13$ ,  $\mu_1 = 1$  (corresponding to Poly-methylpentene) and is embedded in vacuum ( $\mu_2 = \varepsilon_2 = 1$ ).

### 3.1. Spontaneous emission rate

In Fig. 2, we plot the frequency dependence of the radiation efficiency  $F_{sc}$  for an emitter localized at  $\rho_s = 40$  nm,  $\phi_s = 0$  (on the  $\hat{x}$  axis) for  $\mu_c = 0.5, 0.75$ , and 1 eV. The dipole moment  $\vec{p}_s$  is oriented in the radial direction ( $\alpha = 0$ ) in Fig. 2a–c and in the azimuthal direction ( $\alpha = 90^\circ$ ) in Fig. 2d–f. In Fig. 2a and d, we observe that  $F_{sc}$  is enhanced at frequencies near  $0.887 \mu\text{m}^{-1}$  and  $1.25 \mu\text{m}^{-1}$  corresponding to the dipolar and the quadrupolar plasmon resonances of the graphene wire, respectively. The correspondence between the spectral position of these peaks and the dipolar and quadrupolar plasmon resonances are in very good agreement with the real part of the complex  $\omega_n/c$  ( $n = 1, 2$ ) given in Table 1, with  $\omega_n/c$  representing the complex root of the common denominator in Eqs. (11) and (12). For the numerical calculation of  $\omega_n/c$  we have used a Newton–Raphson method and the same parameters used for curves in Fig. 2. The appearance of these peaks do not depend on the orientation angle  $\alpha$  and, since  $\lambda = 2\pi c/\omega \gg a$ , their spectral position agree well with those obtained from the quasistatic approximation for which the stationary plasmonic mode condition is fulfilled [47,49].

On comparing Fig. 2a–c (d–f), we observe that the dipolar maximum is blue shifted from  $\omega/c = 0.8868 \mu\text{m}^{-1}$  to  $\omega/c = 1.25 \mu\text{m}^{-1}$

when  $\mu_c$  is increased from 0.5 eV to 1 eV. This is consistent with the fact that frequency plasmonic resonances are proportional to  $\sqrt{\mu_c}$  [47,49], i.e., the net effect of the chemical potential increment is to increase the surface charge density on the coated graphene.

Another important quantity plotted in Fig. 2 is the quantum efficiency  $\eta_{SE}$  defined as the radiation to emission ratio,  $\eta_{SE} = F_{sc}/F$ . As shown in Fig. 2a and d,  $\eta_{SE}$  takes a value approximately 0.4 for the dipolar plasmon resonance and a value close to zero for the quadrupolar plasmon resonance. On comparing Fig. 2a–c (d–f), we see that the quantum efficiency is increased from 0.4 to 0.6 at the dipolar resonance frequency when the chemical potential is increased from 0.5 eV to 1 eV whereas it remains near zero for the quadrupolar resonance.

An additional interesting results when the line emitter is located outside the wire is the reduction of the radiation efficiency at a specific frequency. This effect is illustrated in Fig. 2a and d where  $F_{sc}$  takes a value  $\approx 10^{-3}$  at  $\omega/c = 1.014 \mu\text{m}^{-1}$  for  $\alpha = 0$ , and a value  $\approx 10^{-2}$  at  $\omega/c = 0.662 \mu\text{m}^{-1}$  for  $\alpha = 90^\circ$ . The frequency where these minima occur is blue shifted as the chemical potential is increased, as can be seen in Fig. 2.

It is worth noting that the same graphene wire serves to provide an enhancement of the radiation by LSP excitation as well as a strongly reduction of the radiation due to non-radiating states. Non-radiating states have already been found in the case of active coated [39] and metallic [50] nano-particles when its are excited by an electric Hertzian dipole. As explained in [50], these states result from the destructive interference between the source dipole and that induced in the nano-particle. The latter exhibits an  $180^\circ$  phase shift with respect to the field at the resonance frequency. Since the orientation of the induced dipole is opposed to the source dipole above (below) the resonance frequency when the source dipole is radially (azimuthally) oriented, the dip in the radiation curve in Fig. 2 occur at right (left) to the resonance peak.

A comparable effect have previously been obtained in case of graphene coated wires but in the framework of far field scattering, where invisibility states have been found to be responsible of the cloaking mechanism when its are illuminated by a plane wave [48,49]. However, unlike these invisibility states for which the frequency only depends on the geometrical and constitutive parameters of the graphene coated cylinder (within the electrostatics approximation the invisibility frequency corresponds to a minimum of the dipolar amplitude  $|b_1|$  given by Eq. (15) [49]), the frequency of the non-radiating states found here (corresponding to minimum values of the radiated power given by Eq. (20)) depends on the dipole location through  $y_s$  and  $\phi_s$ , a common feature of the interference effects. This fact is illustrated in Fig. 3 where we have plotted the radiating efficiency for  $\mu_c = 0.5$  eV. We observe that, for  $\alpha = 0$  the frequency at which the non-radiating states occurs decreases as the distance between the dipole and the wire is increased. On the contrary, the frequency at which the non-radiating states occurs increases as the distance between the dipole and the wire is increased when  $\alpha = 90^\circ$ . In both cases,  $\alpha = 0$  and  $\alpha = 90^\circ$ , the non-radiating state frequency approaches to the dipolar resonance frequency  $\omega_1$  (at which  $F_{sc}$  is enhanced) as the distance between the dipole and the wire is increased. This fact can be readily understood supposing without loss of generality that the emitter is placed on the  $\hat{x}$  axis,  $\phi_s = 0$ , with its dipole moment horizontally oriented,  $\alpha = 0$ . Since the size of the wire is small compared to the wavelength ( $a \ll \lambda = 2\pi/(\omega/c)$ ), we can use the quasistatic approximation. Within this approximation, by retaining only the term of the lowest order in Eq. (8), the scattered magnetic field can be written as

$$\varphi_s^{(2)}(\rho, \phi) = 2ib_1 H_1^{(1)}(k_2 \rho) \sin \phi, \quad (27)$$

where we have taken into account that  $b_1 = b_{-1}$  when  $\alpha = \phi_s = 0$ . If we compare this expression with that corresponding to a point

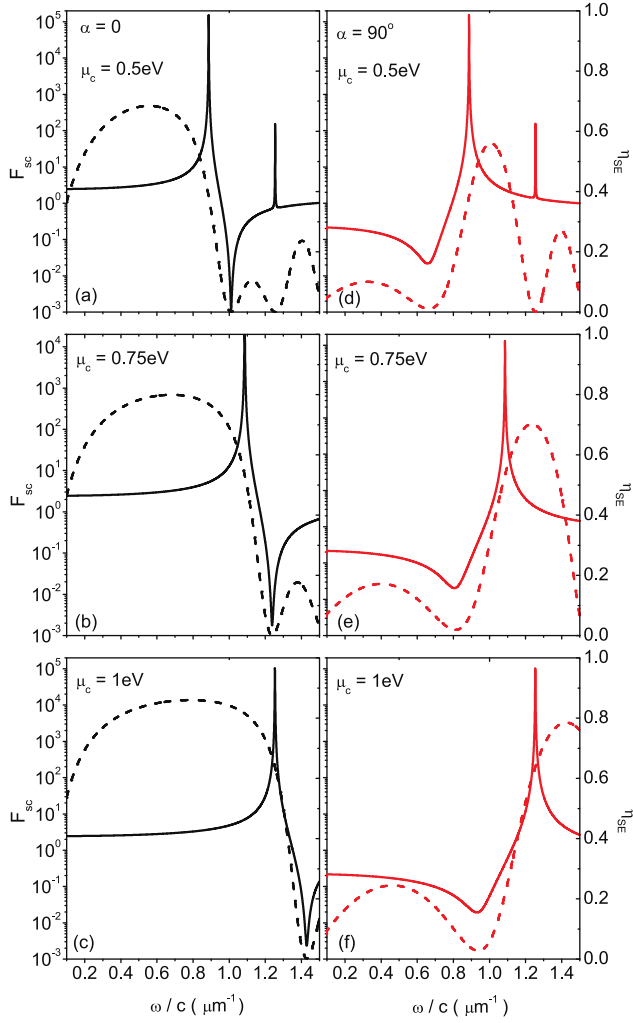


**Fig. 2.** Radiation and quantum efficiencies for a dipole emitter on the  $\hat{x}$  axis placed at a distance of 40 nm from the center of the graphene-coated wire. Radius  $a = 30$  nm, constitutive parameters  $\varepsilon_1 = 2.13$  and  $\mu_1 = 1$  in a vacuum. The curves were calculated for  $\alpha = 0^\circ$  (a)–(c), and for  $\alpha = 90^\circ$  (d)–(f). The graphene parameters are  $T = 300$  K and  $\gamma_c = 0.1$  meV and  $\mu_c = 0.5$  eV (a) and (d), 0.75 eV (b) and (e), 1 eV (c) and (f).

dipole emitter placed at the origin of coordinates with its dipole moment  $p_{ind}$  along the  $\hat{x}$  axis [36],

$$\varphi(\rho, \phi) = \pi k_0 k_2 p_{ind} H_1^{(1)}(k_2 \rho) \sin \phi, \quad (28)$$

it follows that the dipole induced in the wire is given by

$$p_{ind} = p \frac{H_2^{(1)}(k_2 \rho_s) + H_0^{(1)}(k_2 \rho_s)}{\pi} \tilde{b}_1, \quad (29)$$

where  $p$  is the dipole moment of the source emitter. Since the Hankel functions decrease with the argument  $k_2 \rho_s$ , in particular  $H_n^{(1)}(k_2 \rho_s) \approx \sqrt{\frac{2}{\pi k_2 \rho_s}}$  in the limit of large argument, the value of  $p_{ind}$  decreases, eliminating the destructive interference, unless the amplitude  $\tilde{b}_1$  increases which happens if the frequency approaches the resonance.

In the previous examples we have chosen the chemical potential  $\mu_c \gg k_B T$  ( $T$  values less than  $\approx 800$  K), a condition that leads to an intraband term  $\sigma^{intra}(\omega)$  which does not depend on the temperature. Since the resonances occur at a frequency  $\omega \ll \mu_c/\hbar$ , the interband term  $\sigma^{inter}(\omega)$  contribution is negligible compared to that of the intraband term and, consequently, the shape of the calculated curves in Fig. 2 is almost independent on the temperature.

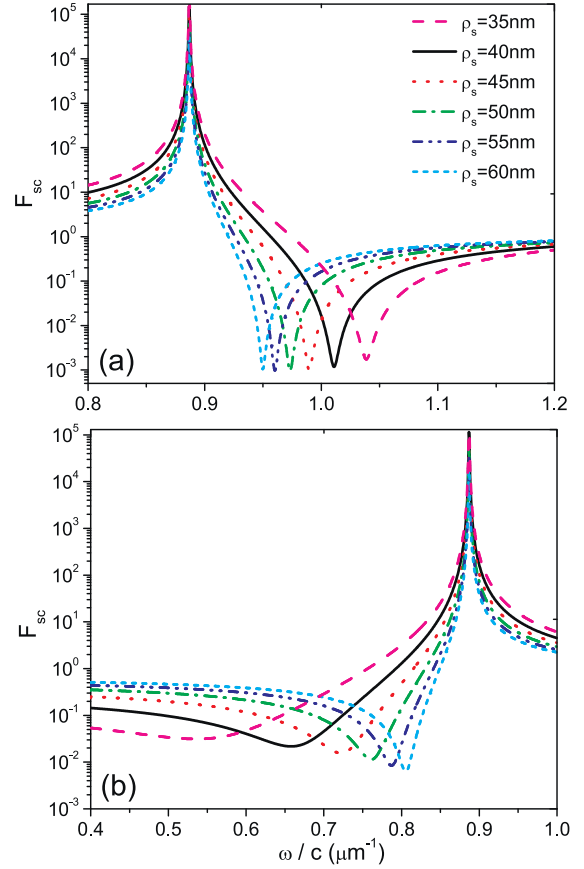


**Fig. 3.** Radiation efficiency curves, calculated for various locations of the dipole source and for  $\alpha = 0^\circ$  (a),  $\alpha = 90^\circ$  (b). The chemical potential  $\mu_c = 0.5$  eV and all other parameters are the same as in Fig. 2.

By decreasing the chemical potential  $\mu_c$ , the temperature effects begin to be significant as can be seen in Fig. 4 where we have plotted  $F_{sc}(\omega)$  and  $\eta(\omega)$  efficiencies for  $\mu_c = 0.1$  eV. The emitter is localized at  $\rho_s = 40$  nm on the  $\hat{x}$  axis with its dipole moment oriented in the radial direction in Fig. 4a and in the azimuthal direction in Fig. 4b. We observe that even though the efficiency curves for  $T \neq 0$  still resembles the efficiency curve for  $T = 0$ , a significant reduction (near three orders of magnitude) in the maximum value reached at the dipolar resonance take place when  $T$  is increased from 0 to 800 K.

### 3.2. Resonance energy transfer rate

In Fig. 5 we plot the frequency dependence of the normalized energy transfer rate  $F_{ET}$  for  $\mu_c = 0.5$  eV (Fig. 5a),  $\mu_c = 0.75$  eV (Fig. 5b) and  $\mu_c = 1$  eV (Fig. 5c) when both the donor and the acceptor dipoles are on the  $\hat{x}$  axis, one of them (the donor) at  $x = -40$  nm and the other (the acceptor) at  $x = 40$  nm ( $\rho_s = \rho_v = 40$  nm and  $\phi_s = 180^\circ$ ,  $\phi_v = 0$ ). The solid line curves were calculated with both the donor and the acceptor dipole moments on the radial direction (in the  $\pm \hat{x}$  axis direction), whereas the dashed line curves were calculated with both dipole moments in the azimuthal direction (in the  $\hat{y}$  axis direction). We observe that at frequencies corresponding to the dipolar and the quadrupolar resonances (only in Fig. 5a the quadrupolar frequency fall in the plotted frequency range), whose values correspond to the real part of the complex roots listed in the second and third column of Table 1, the energy transfer is enhanced near  $10^6 - 10^7$  times the corresponding value to the same dipole pair localized in the unbounded medium 2 (without the graphene wire). Another particular result plotted in

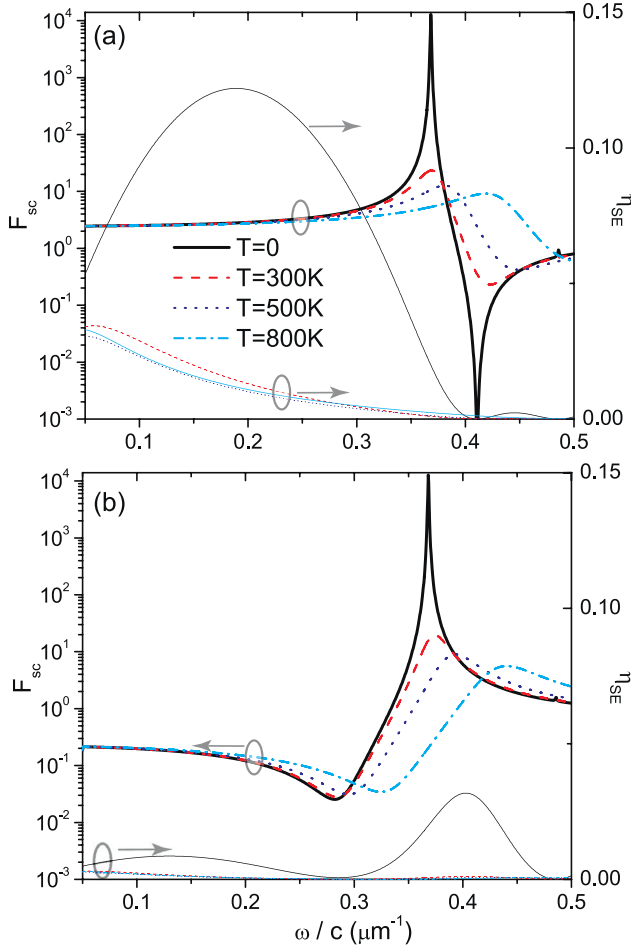


**Fig. 4.** Radiation and quantum efficiencies for a dipole emitter on the  $\hat{x}$  axis placed at a distance of 40 nm from the center of the graphene-coated wire. The curves were calculated for  $\alpha = 0^\circ$  (a), and for  $\alpha = 90^\circ$  (b). The graphene parameters are  $\gamma_c = 0.1$  meV and  $\mu_c = 0.5$  eV and  $T = 0, 300, 500,$  and  $800$  K.

Fig. 5 is a notable reduction of the energy transfer rate at a specific frequency when both dipoles are azimuthally oriented. This fact can be seen in Fig. 6a where we have plotted the transfer rate  $F_{ET}$  for various values of  $\rho_s$  and for  $\mu_c = 0.5$  eV. The acceptor is diametrically opposite to the donor,  $\rho_v = \rho_s$  and  $\phi_s = 180^\circ$ ,  $\phi_v = 0$ . From this figure we observe that the frequency at which the reduction of energy transfer occur depends on  $\rho_s$ , i.e., on the location of the dipole pair. Moreover, the dip in the  $F_{ET}$  curve is blue shifted to the upper limit imposed by the resonance frequency as the distance between dipoles (donor and acceptor) is increased.

The strong reduction in the energy transfer for azimuthal polarization can be understood as an interference process occurring between the fields of the source dipole and the fields produced by the induced dipole in the wire. To illustrate, we consider a simplified scheme consisting in two dipoles, one of them  $p$  corresponds to the source emitter placed at  $x = -\rho_s$  and the other  $p_{ind}$  corresponds to the induced dipole in the wire which is placed at  $x = 0$  (see inset in Fig. 6b). Within the quasistatic approach the magnetic field scattered by the wire (8) is written as

$$\varphi_s^{(2)}(\rho, \phi) = 2b_1 H_1^{(1)}(k_2 \rho) \cos \phi, \quad (30)$$

where we have taken into account that  $b_1 = -b_{-1}$  when  $\alpha = \pi/2$  and  $\phi_s = \pi$ . By comparing this expression with that corresponding to a point dipole emitter placed at the origin of coordinates with its dipole moment  $p_{ind}$  along the  $\hat{y}$  axis [36],

$$\varphi(\rho, \phi) = -\pi k_0 k_2 p_{ind} H_1^{(1)}(k_2 \rho) \cos \phi, \quad (31)$$

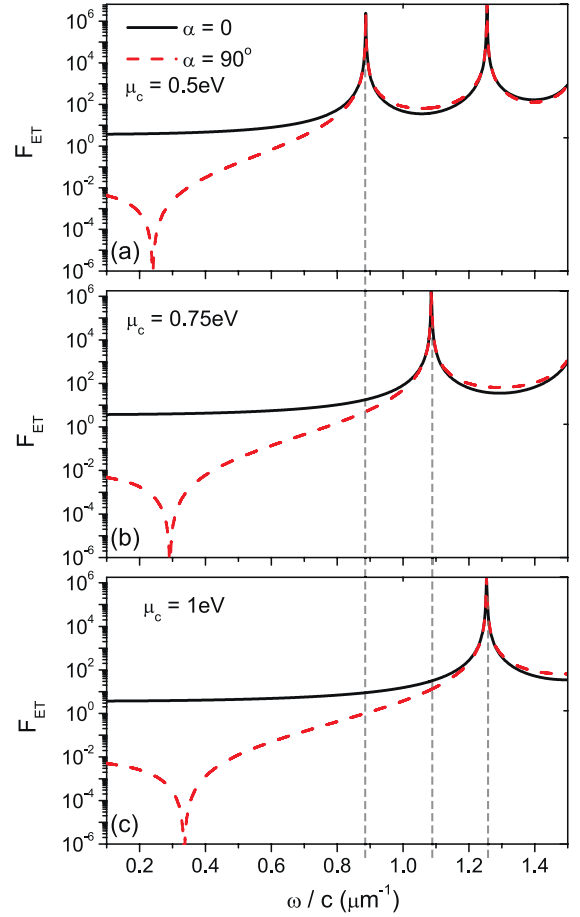


**Fig. 5.** Energy transfer efficiency for a graphene-coated wire with a radius  $a = 30$  nm, constitutive parameters  $\epsilon_1 = 2.13$  and  $\mu_1 = 1$  in a vacuum. The donor and acceptor dipoles are placed diametrically opposed on the  $\hat{x}$  axis at a distance of 40 nm from the center of the graphene wire. The orientation angles are  $\alpha_s = \alpha_v = \alpha = 0^\circ$  (continuous line), and  $\alpha_s = \alpha_v = \alpha = 90^\circ$  (dashed line). The graphene parameters are  $T = 300$  K,  $\gamma_c = 0.1$  meV and  $\mu_c = 0.5$  eV (a),  $0.75$  eV (b),  $1$  eV (c).

it is follows an expression for the dipole induced in the wire

$$p_{ind} = -\frac{2b_1}{\pi k_0 k_2} = -p \frac{H_2^{(1)}(k_2 \rho_s) - H_0^{(1)}(k_2 \rho_s)}{\pi} \tilde{b}_1, \quad (32)$$

where  $p$  is the dipole moment of the source emitter placed at  $x = -\rho_s$ . For distances  $\rho_s$  between dipoles (or from the induced dipole to the observation point) much smaller than the wavelength ( $k_2 \rho_s \ll 1$ ), as that in the inset in Fig. 6a,  $|H_2^{(1)}(k_2 \rho_s)| \ll |H_0^{(1)}(k_2 \rho_s)|$  [40] and as a consequence the induced dipole can be approximated by

$$p_{ind} = -p \frac{H_2^{(1)}(k_2 \rho_s)}{\pi} \tilde{b}_1 = \frac{4\pi i}{\pi^2} \frac{1}{k_2^2 \rho_s^2} \tilde{b}_1, \quad (33)$$

where in the last equality we have used the small argument asymptotic expansions for Hankel functions [40],  $H_2^{(1)}(z) \approx -\frac{4i}{\pi z^2}$ . We now calculate the  $y$ -component of the electric field ( $E_y$ ) produced by this induced dipole at an observation point on the  $\hat{x}$  axis localized at  $x = \rho_s$ . By using the Ampere–Maxwell Eq. (4) the relation between the azimuthal component of the electric field  $E_\phi$  and the  $z$ -component of the magnetic field  $\varphi$  is derived,  $E_\phi = -\frac{i}{k_0 \epsilon_2} \frac{\partial \varphi}{\partial \rho}$  and, since  $\hat{\phi} = \hat{y}$  on the observation point, it follows that  $E_y = E_\phi$ . Taking into account that the distance from the induced dipole to the observation point is much smaller than the wavelength,  $k_2 \rho_s \ll 1$ , and that the polar angle at the observation point  $\phi = 0$ ,

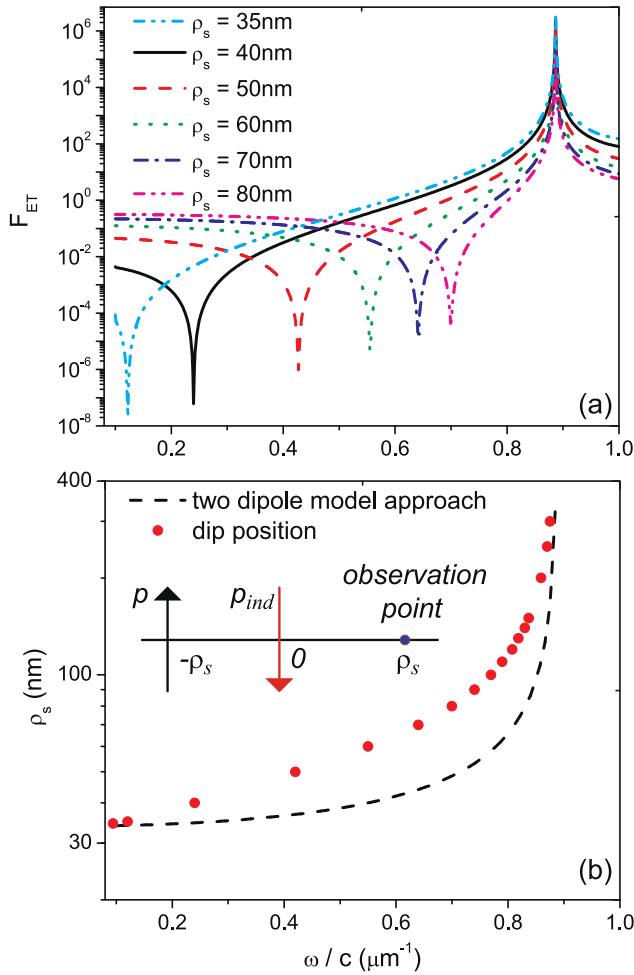


**Fig. 6.** (a) Energy transfer efficiency calculated for both dipoles (donor and acceptor) on the  $\hat{x}$  axis and for  $\alpha_D = \alpha_A = 90^\circ$ . The acceptor dipole is placed diametrically opposed to the donor ( $\rho_D = \rho_A$ ,  $\phi_D = 180^\circ$ ,  $\phi_A = 0$ ). (b) Curves represent the two dipole model values, scatter symbols represent values estimated from the minima in the curves calculated with the Mie theory, such as those shown in Fig. 6a. The inset shows a scheme of the two dipole model, where  $p$  is the dipole moment of the source emitter,  $p_{ind}$  is the induced dipole in the wire which is parallel to the driving field at frequencies less than that of resonance. The chemical potential  $\mu_c = 0.5$  eV and all other parameters are the same as in Fig. 5.

we obtain

$$E_y^{(wire)} = \frac{2p_{ind}}{\varepsilon_2 \rho_s^2}. \quad (34)$$

In a similar way, the  $y$ -component of the electric field at  $x = \rho_s$  produced by the primary dipole placed at  $x = -\rho_s$  is

$$E_y^{(emitter)} = \frac{2p}{\varepsilon_2 (2\rho_s)^2}, \quad (35)$$

and the  $y$ -component of the total electric field is given by superposition of the fields (34) and (35). By requiring this field be equal to zero and using Eq. (33) we obtain

$$\frac{1}{k_2^2 x_s^2} = -\frac{\pi}{4k_2^2 a^2} \left[ \frac{\varepsilon_2 + \varepsilon_1 + \frac{4\pi\sigma i}{ck_0 a}}{\varepsilon_2 - \varepsilon_1 - \frac{4\pi\sigma i}{ck_0 a}} \right], \quad (36)$$

where we have used the small argument asymptotic expansions for Bessel and Hankel functions [40] in the calculation of the amplitude  $b_1$  given by Eq. (15). As  $\hbar\omega$  is small enough compared with  $\mu_c$ , the intraband contribution dominates and the graphene conductivity follows a Drude model dispersion. This fact provides an

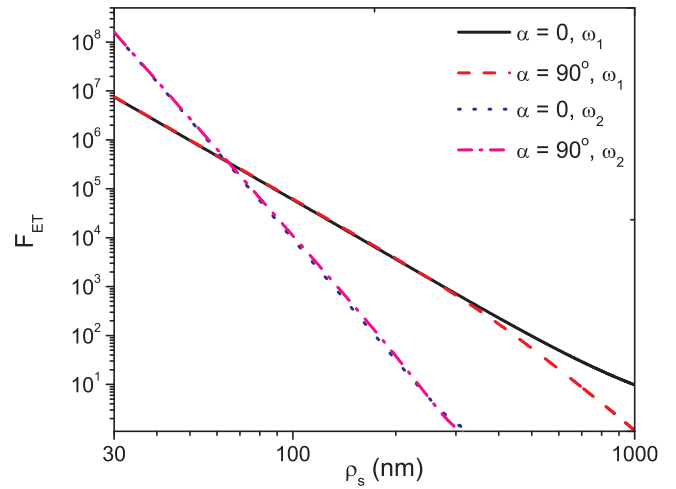


**Fig. 7.** Normalized energy transfer as a function of  $\rho_s$  for  $\mu_c = 0.5$  eV. The donor and the acceptor are placed diametrically opposed ( $\rho_D = \rho_A$ ) on the  $\hat{x}$  axis and the orientation angles are  $\alpha_D = \alpha_A = \alpha = 0^\circ$ ,  $\alpha_D = \alpha_A = \alpha = 90^\circ$ . The donor frequency is chosen to be the resonance plasmon frequency,  $\omega_1/c = 0.8868 \mu\text{m}^{-1}$  and  $\omega_2/c = 1.2547 \mu\text{m}^{-1}$ . All other parameters are the same as in Fig. 5.

almost purely imaginary graphene conductivity. In the ideal lossless case Eq. (36) has real solutions and it determines  $\rho_s$  as a function of frequency  $\omega$ , i.e., the positions of the donor ( $x = -\rho_s$ ) and the acceptor ( $x = \rho_s$ ) dipoles (both symmetrically located with respect to the graphene wire) for which the energy transfer from the donor to the acceptor is null.

In Fig. 6b we plotted the solutions of Eq. (36) with a dashed line and the values indirectly estimated from the observation of positions of minima in energy transfer spectra calculated with the Mie theory with circles. Since Eq. (36) was obtained within the approximation  $k_2 \rho_s \ll 1$ , the two dipole model given by Eq. (36) agree well with the Mie theory only for very low frequencies. However, despite the fact that for higher frequencies the dashed curve in Fig. 6b appreciably departs from the circles curve, both curves present the same qualitative characteristics indicating that the simple two dipole model reproduces the behavior of the near zero energy transfer condition.

In order to study the behavior with the distance to the wire we vary the donor and the acceptor positions on the  $\hat{x}$  axis maintaining both dipoles at the same  $|x|$ , i.e.,  $\rho_D = \rho_A$  and  $\phi_D = 180^\circ$ ,  $\phi_A = 0$ . The normalized factor  $F_{ET}$  as a function of  $\rho_s$  is plotted in Fig. 7 for  $\mu_c = 0.5$  eV. The donor frequency is chosen to be the resonance plasmon frequency,  $\omega_1/c = 0.8868 \mu\text{m}^{-1}$  and  $\omega_2/c = 1.2547 \mu\text{m}^{-1}$ . We can see that all the curves are exponentially decreasing as the  $\rho_s$  value is increasing, i.e. as the distance  $d = 2\rho_s$  between donor and acceptor dipole moments is increasing. In particular, for  $\rho_s < 60$  nm (near field interaction) the quadrupolar plasmon resonance yields a larger energy transfer comparing with that corresponding to the dipolar resonance. However, for  $\rho_s > 60$  nm ( $d > 120$  nm) the quadrupolar energy transfer decays quickly in comparison with that corresponding to the dipolar resonance.

To calculate the dependence of the energy transfer rate on the temperature we choose  $\mu_c = 0.1$  eV. In Fig. 8 we observe that the frequency at which the energy transfer is enhanced is blue shifted and that the maximum value reached at these frequencies is reduced as the temperature is increased. For instance, we observe that the dipolar maximum is decreased near three orders of magnitude and that the frequency at which this occur is blue shifted from  $\omega/c \approx 0.37$  to  $\omega/c = 0.43$  when  $T$  is increased from 0 to 800 K.

It is well established that the energy transfer process is usually quantified by the efficiency  $\eta_{ET}$  defined as the ratio between the relative contribution of the energy transfer process to the total

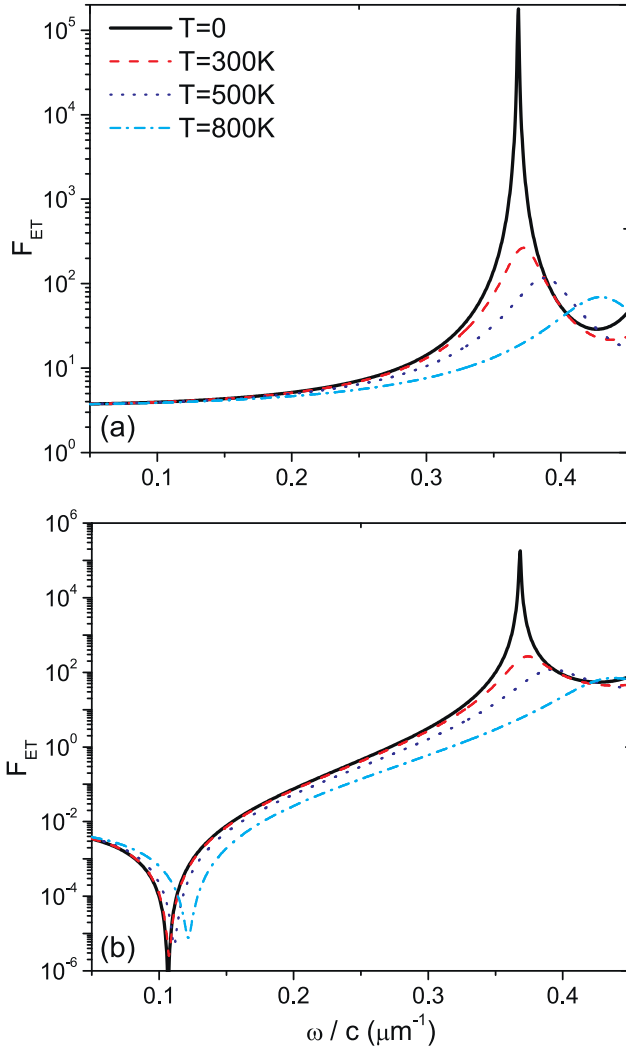


**Fig. 8.** Energy transfer efficiency for a graphene-coated wire with a radius  $a = 30$  nm, constitutive parameters  $\epsilon_1 = 2.13$  and  $\mu_1 = 1$  in a vacuum. The donor and acceptor dipoles are placed diametrically opposed on the  $\hat{x}$  axis at a distance of 50 nm from the center of the graphene wire. The orientation angles are  $\alpha_s = \alpha_v = \alpha = 0^\circ$  (a), and  $\alpha_s = \alpha_v = \alpha = 90^\circ$  (b). The graphene parameters are  $\gamma_c = 0.1$  meV,  $\mu_c = 0.1$  eV and  $T$  is varied.

decay rate of the donor,

$$\eta_{ET} = \frac{F_{ET}}{F_{ET} + F}. \quad (37)$$

From this expression, it follows that the efficiency  $\eta_{ET}$  depends on the ratio between the energy transfer to the relaxation energy into nonradiative modes and photons,  $\gamma = F_{ET}/F$ , that is, on the energy transfer rate normalized with respect to the donor decay rate  $F$ . In Fig. 9 we plot the spatial distribution of  $\gamma$  as a function of the acceptor location for  $\mu_c = 0.5$  eV. The position of the donor is fixed on the  $\hat{x}$  axis at  $\rho_s = 40$  nm,  $\phi_s = 0$  and is indicated with an arrow. The orientation of the donor and the acceptor dipole moments is radial. The color map is calculated for the acceptor placed in each point of the plot. Fig. 9a was calculated for  $\omega/c = 0.886 \mu\text{m}^{-1}$  at which the dipolar resonance occur and Fig. 9b was calculated for  $\omega/c = 1.254 \mu\text{m}^{-1}$  at which the quadrupolar resonance occur. In the first case the map appear enhanced in two opposite regions on the cylindrical section where  $\gamma$  reaches values close to 1. It is follows that, in these regions, the decay of the excited state of the donor occur into the two ways, by energy transfer to the acceptor and by relaxation into LSP or photons, with almost the same

rate. We see that the  $\gamma$  map takes a value close to zero on points near the  $x = 0$  line. This is explained by taking into account that at resonant frequency the electric field is almost in the azimuthal  $\hat{\phi}$  direction on this line whereas the acceptor is placed with its dipole moment in the radial  $\hat{r}$  direction. Therefore, the numerator in Eq. (24) is close to zero.

Fig. 9b shows four zones on the cylindrical section in which the  $\gamma$  function is enhanced. These zones appear limited by two lines,  $y = \pm x$ , where the electric field is in the azimuthal direction at the quadrupolar resonant frequency. As a consequence the energy transfer to the acceptor positioned at these lines with its dipole moment along the radial direction is zero as can be seen in Fig. 9b.

Similar maps have been observed (not shown in Fig. 9) when both the donor and the acceptor dipoles are placed along the azimuthal direction.

Fig. 10 shows the transfer efficiency  $\eta_{ET}$  as a function of the radial position of the acceptor diametrically opposite to the donor for  $\mu_c = 0.5, 0.75,$  and  $1$  eV. The donor is fixed at  $\rho_s = 40$  nm and the position of the acceptor  $\rho_v$  is varied in the range 30 nm to 1  $\mu\text{m}$ . As is indicated in Fig. 10, each curve was calculated at the corresponding resonance frequency. We see that the efficiency  $\eta_{ET}$  curves reach its maximum value at the graphene coating and it is exponentially decreasing as  $\rho_v$  is increasing. Moreover, the values of  $\eta_{ET}$  decreases as  $\mu_c$  is increased.

#### 4. Conclusions

The scattering problem of a dipolar line emitter in the proximity of a graphene coated wire of circular cross section was theoretically studied by applying an analytical method based on the separation of variables approach.

We calculated the radiation decay rate and the quantum efficiency as a function of frequency for various values of the chemical potential. In the presented examples, we have varied the location and the orientation of the dipole moment of the source emitter. Both orientations radial and azimuthal couple to LSPs in the graphene coating leading to a strongly enhancement of the spontaneous decay rates. The correspondence between the spectral peak positions and the multipolar SP resonances (dipolar and quadrupolar in this work) has been shown by calculating the complex poles of the coefficients of the multipole expansion of the electromagnetic field.

An interesting result revealed in this study is the appearance of a pronounced reduction in the power radiated by the emitter coupled to the graphene wire, which is manifested by a dip in the radiation efficiency. Unlike the resonance peaks at which the radiation is enhanced, whose frequencies are determined by structural parameters (geometrical and constitutive), the frequency of the non-radiating states also depends on the dipole location, *i.e.*, the dip appears at different frequencies for different distances from the emitter to the graphene wire. For the radial orientation the dip occur at a frequency greater than that corresponding to the dipolar resonance  $\omega_1$  and for the azimuthal orientation the dip occur at a frequency lower than  $\omega_1$ .

We also calculated the energy transfer between two line dipole emitters in the proximity of the graphene wire. Our calculus shows that the efficiency of the energy transfer is enhanced up to 7 orders of magnitude at SP resonance frequencies. Even though the energy transfer  $F_{ET}$  takes similar values near the resonance frequencies regardless the dipole moment orientations ( $\hat{r}$  or  $\hat{\phi}$  orientations),  $F_{ET}$  curves are deeply dependent on these orientations for other frequencies. For instance, the efficiency  $F_{ET}$  is strongly reduced at a specific frequency depending on the position of the source emitters when they are oriented in the azimuthal direction. Moreover, the dip in the  $F_{ET}$  curve is blue shifted as the distance

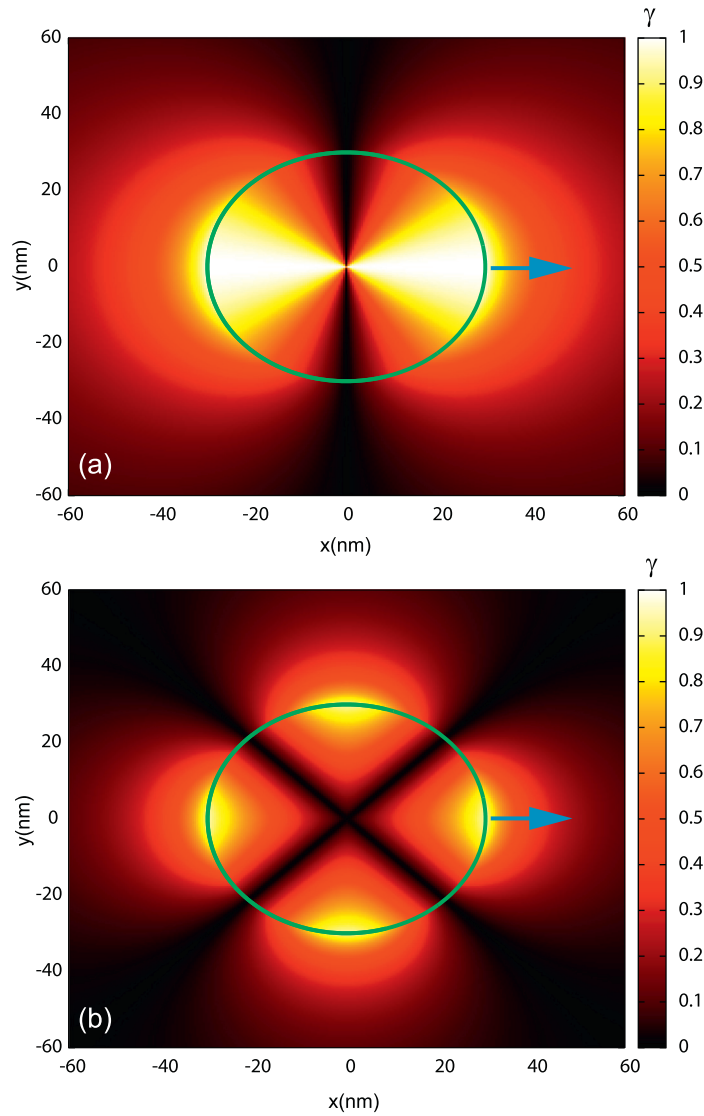


**Fig. 9.** Spatial distribution of  $\gamma$  as a function of the acceptor location. The donor position is fixed on the  $\hat{x}$  axis at  $\rho_s = 40$  nm. The donor and acceptor dipole moments are oriented in the radial direction. The donor frequency is chosen to be the resonance plasmon frequency  $\omega_1/c = 0.8868 \mu\text{m}^{-1}$  (a) and  $\omega_2/c = 1.2547 \mu\text{m}^{-1}$  (b). The chemical potential  $\mu_c = 0.5$  eV and all other parameters are the same as in Fig. 5.

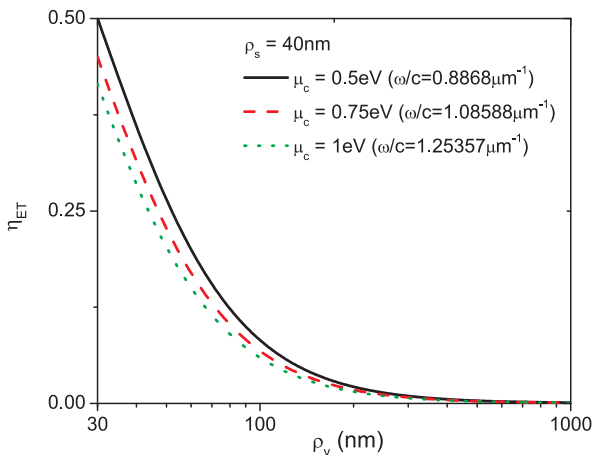


**Fig. 10.** Energy transfer efficiency  $\eta_{ET}$  as a function of the radial position of the acceptor  $\rho_v$  for  $\mu_c = 0.5, 0.75,$  and  $1$  eV. The donor position is fixed at  $\rho_s = 40$  nm diametrically opposite to the acceptor.

between dipoles is increased. On the other hand, non such reduction is observed for the radial orientation.

Our calculus shown that, by dynamically tuning the chemical potential of graphene, the spectral region where the energy transfer as well as the emission–radiation efficiencies is enhanced (or reduced) can be chosen over a wide range.

It is known that a graphene layer can supports  $s$  polarized surface plasmons [45] which are weakly bound and exhibit a very low propagation loss [51], *i.e.*, the absorption of these plasmons is weak [52,53], even in a coupling condition [54]. In the context of this paper, these modes would be excited by an infinitely long oscillating current (along the wire axis) which has not much to do with the emission from a dipole source. We are planning to report the results of such study in a future paper considering a point like dipole source with its dipole moment along the  $z$  axis.

#### Acknowledgments

The author acknowledge the financial supports of Fundación Universidad de Belgrano (UB) and Consejo Nacional de Investigaciones Científicas y Técnicas, (CONICET, PIP 1800).

## References

- [1] Purcell EM. *Phys Rev* 1946;69:674.
- [2] Carminati R, Caze A, Cao A, Peragut A, Krachmalnicoff V, Pierrat R, Wil D. *Surf Sci Rep* 2015;70:1–41.
- [3] Muskens OL, Giannini V, Sánchez-Gil JA, Rivas JG. *Nano Lett* 2007;7: 2871–5
- [4] Rogobete L, Schniepp H, Sandoghdar V, Henkel C. *Opt Lett* 2003;28:1623–5.
- [5] Tame MS, McEnergy KR, Özdemir K, Lee J, Maier SA, Kim MS. *Nat Phys* 2013;9:329–40.
- [6] Sokhoyan R, Atwater HA. *Optic Express* 2013;21: 32279–90
- [7] Ginzburg P, Roth DJ, Nasir ME, Segovia P, Krasavin AV, Levitt J, Hirvonen LM, Wells B, Suhling K, Richards D, Podolskiy VA, Zayats AV. *Light* 2017;6:e16273.
- [8] Mahmoud AM, Liberal I, Engueta N. *Opt Mater Express* 2017;7:415–24.
- [9] Karanikolas V, Marocico CA, Bradley AL. *Phys Rev A* 2014;89:063817.
- [10] Martín-Cano D, Martín-Moreno L, García-Vidal FJ, Moreno E. *Nano Lett* 2010;10:3129–34.
- [11] Andrew P, Barnes WL. *Science* 2004;306:1002–5.
- [12] Akselrod GM, Argyropoulos C, Hoang TB, Ciraci C, Fang C, Huang J, Smith DR, Mikkelsen MH. *Nat Photonics* 2014;8:835–40.
- [13] Oulton RF, Sorger VJ, Zentgraf T, Ma R, Gladden C, Dai L, Bartal G, Zhang X. *Nature* 2009;461:629–32.
- [14] Akimov AV, Mukherjee A, Yu CL, Chang DE, Zibrov AS, Hemmer PR, Park H, Lukin MD. *Nature* 2007;450:402–6.
- [15] Yang X, Li Y, Lou Z, Chen Q, Li B. *ACS Appl Energy Mater* 2018;1:278–83.
- [16] Jablan J, Soljacic M, Buljan H. *Proc IEEE* 2013;101:1689–704.
- [17] Xia F. *Nat Photonics* 2013;7:420.
- [18] Christensen T. *From Classical to Quantum Plasmonics in Three and Two Dimensions*. Springer; 2017.
- [19] Farmani A, Zarifkar A, Sheikhi MH, Miri M. *Superlattices Microstruct* 2017;112:404–14.
- [20] Moradi A. *J Appl Phys* 2018;123:043103.
- [21] Cheng Y, Yang J, Lu Q, Tang H, Huang M. *Sensors* 2016;16:773.
- [22] Saavedra JRM, de Abajo F J G. *Appl Phys Lett* 2018;112:061107.
- [23] Raether H. *Surface Plasmons on Smooth and Rough Surfaces and on Gratings*. Springer-Verlag Berlin; 1988.
- [24] Maier SA. *Plasmonics: Fundamentals and Applications*. New York: Springer; 2007.
- [25] Cuevas M, Depine RA. *Phys Rev Lett* 2009;103:097401.
- [26] Zeller M, Cuevas M, Depine RA. *JOSA B* 2011;28:2042–7.
- [27] Farmani A, Miri M, Sheikhi MH. *JOSA B* 2017;34:1097–106.
- [28] Cuevas M. *Phys Lett A* 2016;380:4027–31.
- [29] Slipchenko TM, Nesterov ML, Martín-Moreno L, Nikitin AY. *J Opt* 2013;15:114008.
- [30] Ferreira A, Peres NMR. *Phys Rev B* 2012;86:205401.
- [31] Biehs SA, Agarwal GS. *Appl Phys Lett* 2013;103:243112.
- [32] Huidobro PA, Nikitin AY, Gonzalez-Ballester C, Martín-Moreno L, García-Vidal FJ. *Phys Rev B* 2012;85:155438.
- [33] Bian T, Chang R, Leung PT. *Plasmonics* 2016;11:1239–46.
- [34] Karanikolas VD, Marocico CA, Bradley AL. *Phys Rev B* 2016;93:035426.
- [35] Cuevas M. *J Opt* 2016;18:105003.
- [36] Cuevas M. *J Quant Spectrosc Radiat Transfer* 2018;206:157–62.
- [37] Wang W, Li BH, Stassen E, Mortensen NA, Christensen J. *Nanoscale* 2016;8:3809–15.
- [38] Cuevas M. *J Quant Spectrosc Radiat Transfer* 2017;200:190–7.
- [39] Arslanagic S, Ziolkowski RW. *J Opt* 2010;12:024014. (9pp).
- [40] Abramowitz M, Stegun IA. *Handbook of Mathematical Functions*. New York: Dover; 1965.
- [41] Novotny L, Hecht B. *Principles of Nano-Optics*. New York: Cambridge University Press; 2006.
- [42] Martín-Moreno L, de Abajo F J G, García-Vidal FJ. *Phys Rev Lett* 2015;115:173601.
- [43] Merano M. *Phys Rev A* 2016;93:013832.
- [44] Falkovsky FA. *Phys Usp* 2008;51: 887–97
- [45] Milkhailov SA, Siegler K. *Phys Rev Lett* 2007;99:016803.
- [46] Falkovsky LA, Pershoguba SS. *Phys Rev B* 2007;76:153410.
- [47] Cuevas M, Riso M, Depine RA. *J Quant Spectrosc Radiat Transfer* 2016;173:26–33.
- [48] Chen PY, Alu A. *ACS Nano* 2011;5:5855–63.
- [49] Naserpour M, Zapata-Rodríguez CJ, Vukovic SM, Pashaeiadi H, Belic MR. *Sci Rep* 2017;7:12186.
- [50] Mertens H, Koenderink AF, Polman A. *Phys Rev B* 2007;76:115123.
- [51] Mason DR, Menabde SG, Park N. *Opt Express* 2014;22:201871.
- [52] Hanson GW. *J App Phys* 2008;103:064302.
- [53] Merano M. *Opt Lett* 2016;41:2668–71.
- [54] Farmani A, Miri M, Sheikhi MH. *IEEE Photonics Technol Lett* 2017;30:153–6.